The importance of presoaking to improve the efficiency of MgCl2-modified and non-modified biochar in the adsorption of cadmium

Effect of presoaking on kinetics of cadmium (Cd) adsorption on modified and unmodified rice husk biochars

Abstract

In the last two decades, several studies have been conducted on biochar production and optimal conditions for the application of biochar for removing contaminants from the aquatic environments. However, presoaking, as one of the most important physical factors affecting the adsorption behavior of biochar, has not been studied yet. For this, rice husk biochars were produced at 450 and 600 °C, then, prior and after modifications by potassium hydroxide and magnesium chloride treatments, kinetics of cadmium adsorption was studied in background solution-presoaked and non-presoaked biochars. Furthermore, the influence of a variety of environmental parameters including pH, temperature and particle size were investigated. Results revealed that the amount of cadmium adsorbed on the presoaked biochars was significantly higher than that on non-presoaked biochars. The highest cadmium adsorption capacities of the soaked biochars were 98.4, 97.6, and 89.8 mg/g for BMS600 (presoaked magnesium modified at 600 °C), BMS450 (presoaked magnesium modified at 450 °C), and BKS450 (presoaked potassium modified at 450 °C), respectively, much more than those observed for unmodified presoaked biochars (7.6 and 7.5 mg/g for BS450 and BS600, respectively). The modeling of kinetic results showed that in all cases the pseudo-second-order model well-fitted (R^2 > 0.99) the cadmium adsorption data. In conclusion, biochar presoaking significantly increased cadmium adsorption and reduced the equilibrium time, demonstrating an efficient and economic method to increase the removal of contaminants in aquatic environments.

Keywords; Adsorption kinetic, modified biochar, Cadmium removal, presoaking process.

1 Introduction

Today the pollution of water resources with Potentially Toxic Elements (PTE) is receiving great attention (Joseph et al., 2019; Kumar et al., 2021) and several studies have been conducted to reduce the related risks. Various biological, chemical, and physical methods have been proposed for the removal of PTEs from the aqueous media (Ighalo et al., 2020; Cheng et al., 2016; Denng et al., 2021; Oh et al., 2019). Using the biological methods, including bioremediation, phytoremediation and the use of microbs, the goal is either to stabilize or to extract contaminants from the matrix (Rajendran et al., 2022; Khoo et al., 2021). Among physical and chemical methods the most used approaches include adsorption, filtration, oxidation or reduction, ion exchange, and electro synthetic precipitation. Among these methods, adsorption is a very efficient and widely used technique for their removal from water media) Yada and Jadeja, 2021).

Various compounds such as natural polymers (Abdel-Halim and Al-Deyab, 2011), synthetic polymers (Kampalanonwat, and Supaphol, 2014), clay minerals (Coles and Yong, 2002; Liu et al., 2016), active carbon (Monser, and Adhoum, 2002; Yang et al., 2007), organic components (Oliveira et al., 2008; Duan et al., 2018; Dişbudak et al., 2002), nanomaterials, nanotubes (Tian et al., 2012; Wang et al, 2010), and biochar (Ighalo et al., 2022) have been used for the removal of PTEs from aqueous solutions. Among these, biochar is a very interesting choice, as it can be produced from inexpensive or waste feedstocks, it is effective, more environmentally friendly than other adsorbents and it can be used to remove a wide range of contaminants (Shakoor et al., 2020). The use of biochar was firstly described by Corapcioglu and Huang (1987), who evaluated the properties of aqueous activated carbon on the adsorption of Ni (II), Cu (II), Pb (II), and Zn (II), reporting that cations adsorption was controlled by surface area, carbon type, and pH. Subsequently, many studies have been performed to produce biochar from different materials and to remove a wide range of pollutants in aqueous media (Singh et al., 2021; Inyang et al., 2012; Usman et al., 2016).

Biochar characteristics are affected by production conditions and feedstock type (Kloss et al., 2012). The increase of the pyrolysis temperature, for example, causes a decrease of aliphatic chains of the matrix and of cation exchange capacity (CEC), and also an increase of the specific surface area and of aromatic moieties. Rego et al. (2022), by examining the effect of

temperature and pyrolysis time on wheat straw biochar, found that increasing the temperature and pyrolysis time reduced the amount of oxygen and volatiles in the final product. Zhao et al. (2018) evaluated the effect of heating rate, pyrolysis temperature and duration on canola biochar production, concluding that pyrolysis temperature had the greatest effect on biochar pollutant removal performance. In general, specific surface area, ash percentage, and pH, increase with pyrolysis temperature, while yield, volatiles, and oxygen fraction decreases with it. Apart these aspects, also the experimental conditions play an important role in determining the efficiency of the pollutants abatement (Berslin et al., 2021), so several scientists investigated the effect of pH, ionic strength, and ionic competition for PTEs removal in order to reach the best conditions for a very efficient process. Concerning cadmium removal, Park et al. (2017) reported that the highest amount of cadmium adsorption was observed at pH 7 and decreasing the ionic strength to limit the interaction between ions in solution. Similarly, Xiao et al. (2017) found that the highest adsorbed amount was observed at a slightly acidic pHs and low ionic strengths, as in these conditions the electrostatic repulsion between adsorptive and adsorbate decreases, and the proton competition is limited.

Physical separation of biochar particles from aqueous solutions has constantly been one of the most important challenges in the application of biochar in the aquatic media. Magnetization has been proposed as an efficient method to solve this problem, as in the functionalization of rice straw biochar with iron compounds (Huang et al., 2021).

Although all these conditions are fundamental to achieve good results in water depollution applications, a last important factor needs to be considered: the possibility to favor the physical contact of biochar with aqueous solutions, in fact, the adsorption of ions on biochar demands an intimate contact of the solid phase with the liquid phase (Brown et al., 1969). Biochar is a porous and partially hydrophobic material (Gray et al., 2014) and to achieve the best adsorption conditions, the solution needs to reach not only the external but also the internal (in the pores) surface (Brown et al., 1969). In addition, the surface character can affect the rate of adsorption, and with a proper affinity, the equilibrium of the adsorption process can occur in a shorter time (Brown et al., 1969) allowing to reduce cost and process time. Given these premises, this study was conducted to investigate: 1- the effect of biochar presoaking on Cd adsorption kinetics in

modified and unmodified biochar, 2 -the effect of pH, particle size, and temperature on the presoaking process.

2 Material and methods

2.1 Biochar production and modification

The rice husks were obtained from Astana rice processing factory (Gillan province, Iran), passed through a 10-mesh sieve and dried at 70 °C for 24 hours. To produce biochar modified with magnesium chloride (BM) and potassium hydroxide (BK), dry rice husks were soaked at a 1 to 5 ratio (500 g of rice husk in 2.5 L of solution) in 1 M $MgCl_2$ and KOH solutions, stirred for 24 h and dried at 70°C for 48 h. Original and treated rice husks were then heated in a muffle oven at 450 or at 600 °C in oxygen-free conditions under argon flow (10 cm^3/min) for 2 hours. After cooling, the biochars were washed with distilled water 10 times to remove residual base cations and after each step, electrical conductivity (EC) was measured until value of EC < 1.5 dS/m was reached. Finally, modified and unmodified biochars were dried and passed through, respectively, a 100 or a 500 µm sieve and kept in closed containers for further experiments.

Table 1

Biochar types used in this experiment

Biochar type	modification	Pyrolysis temperature
B600	-	600 °C
B450	-	450 °C
BM600	$MgCl_2$	600 °C
BM450	$MgCl_2$	450 °C
BK450	KOH	450 °C

2.2 Biochar characterization

For pH and electrical conductivity (EC) analysis, 5 g of biochar were suspended in 50 ml of deionized water and shaken at 120 rpm for 24 hours. After shaking, the pH of the suspensions

was measured immediately, whereas EC was measured after 20 minutes without further shaking. To determine the ash content, samples were dried at 105 °C and weighed, then heated for 6 hours in a muffle oven at 750 °C in the presence of air. Finally, the weight of residues was measured, and the percentage of ash was determined from the following equation (Eq. (1)) (Sinegh et al., 2017).

$$(1)\ \%\ \text{Ash} = \frac{weight_{\,residue\ after\ 750\ °C}}{weight_{150\ °C\ dried}} \times 100$$

The total Cd content in the biochar samples was determined using the method reported by Sinegh et al. (2017). Briefly, 0.2 g of biochar were placed in a digestion tube. Then, samples were heated at 650 °C for 8 h. After cooling, 4 ml of HNO_3 were added to the samples and heated at 120 °C for 2 hours, afterward 4 ml of H_2O_2 and 1 ml of HNO_3 were added to tubes and heated at 80 °C for 2 hours. After digestion, HCl 6 M was added to tubes and held at room temperature for 24 h. Finally, the samples were filtered (Whatman n. 41) and the concentration of the elements was measured using ICP-MS (PerkinElmer NexION® 350D).

Pore volume and surface area of biochar samples were measured via N_2 adsorption-desorption gas-volumetric analysis at nitrogen boiling point (Micromeritics ASAP 2020 Plus). The pH of the point of zero charge (pH_{pzc}) was measured using the Faria and Pereira (2004) method. In brief, 0.15 g biochar was added to closed 100 ml Erlenmeyer flasks containing 50 ml 0.01 M $NaNO_3$ with pH adjusted between 2 and 12. The final pH was determined after stirring for 48 h at 25°C. The pH_{pzc} is the point on the curve where the final pH is equal to the initial pH. Fourier transform infrared (FTIR) was used to determine the functional groups using a Vector 22 by Bruker, equipped with Globar lamp and DTGS detector and considering 128 scans with a resolution of 4 cm^{-1} in the range 400-4000 cm^{-1}. The total content of carbon, nitrogen, and hydrogen in the biochar samples was determined using an elemental analyzer (Elementar UNICUBE). The physical properties and morphology of the surface were evaluated using scanning electron microscopy (SEM-EDX) with a ZEISS EVO 50 XVP with LaB_6 source, equipped with detectors for secondary electrons collection and an Energy Dispersive X-ray Spectrometry (EDS) probe for elemental analyses. Samples were covered with a chromium layer of ~5 nm of

thickness before the analysis to prevent charging (Emitech K575X sputter coater equipped with a film thickness monitor and Cr target).

Adsorption experiments

The kinetic experiments were conducted on (S) presoaked and (NS) non-presoaked adsorbents. During the presoaking process, 10 ml of background solution ($NaNO_3$ 0.01 M, pH 6) was added to centrifuge tubes containing 0.5, or 0.2 g of unmodified or modified biochars, respectively, and left in contact for 0.5, 1, 2, 4, 8, 16, 24, 48, and 168h. After this step, 10 ml of a Cd solution at pH 6 (400 mg/l of Cd in the case of unmodified biochars and 2000 mg/l in the case of modified biochars) were added and the samples were shaken at room temperature (25 ± 1°C) for 0.5, 1, 2, 4, 8, 16, 24, 48, and 168 h. The same process was repeated also for non-presoaked biochars, with 0.5 or 0.2 g of unmodified or modified biochars placed in centrifuge tubes containing 20 ml of Cd solution (200 mg/l of Cd for unmodified biochar experiment and 1000 mg/l for modified biochar experiment) and shaken for different times at 25 ± 1°C.

To investigate the effect of temperature and pH on Cd adsorption kinetics in unmodified biochars, suspension pH was adjusted to 2, 5, and 6 and shaken at 15 ± 1, 25 ± 1, and 35 ± 1°C for the previously mentioned contact times. After each contact time, presoaked and non-presoaked samples were centrifuged (at 4000 rpm), filtered (Whatman n. 41) and the residual concentration of Cd in the solution was determined by ICP-MS. Adsorbed Cd was calculated from the difference between the initial concentration and the equilibrium concentration. Finally (Eq. (2)) pseudo-first-order, (Eq. (3)) pseudo-second-order, and (Eq. (4)) Intraparticle diffusion models were used to model Cd adsorption kinetics:

(2) $\log (q_e - q_t) = \log q_e - \frac{k_1}{2.0303} t$ (Lagergren, 1898)

(3) $\frac{t}{qt} = \frac{1}{k_2 q_e^2} - \frac{t}{q_e}$ (Ho and McKay, 1999)

(4) $q_t = k_d t^{1/2} + c$ (Weber and Morris, 1963)

Where q_e, c, and q_t are the amounts of Cd (mg/g), adsorbed respectively at the equilibrium, at time zero, and at time t (h) respectively, k_1, k_2, and k_d the rate of constant of pseudo-first-order (1/h), pseudo-second-order (g/mgh), and intraparticle diffusion (mg/g$h^{0.5}$), respectively.

3 Results and discussion

3.1 Biochar characterization

The main characterization results are reported in Table 2. For what concerns the composition, as the pyrolysis temperature increased, the carbon content increased, whereas the % O and % H, and the atomic ratio H/C and O/C decreased, indicating loss of hydrogen and oxygen from the matrix during the pyrolysis treatment activated by temperature. In the modified biochars, the amount of oxygen and hydrogen ratios were significantly higher than in the unmodified biochars. According to the FTIR analysis (Fig. 1), presented below, the increase in oxygen and hydrogen content can be attributed to the formation of hydroxyl and carboxyl functional groups in the biochars during the modification process.

Table 2

Properties of modified and unmodified rice husk biochars.

Parameter	BM600	BM450	BK450	B600	B450
C (%)	38.0	41.2	51.9	53.5	50.5
H (%)	2.7	3.8	4.3	1.7	2.8
O (%)	18.4	20.6	19.2	12.1	16.2
H/C	0.071	0.093	0.082	0.032	0.056
O/C	0.48	0.49	0.37	0.27	0.32
pH (1:10)	8.6	8.2	9.0	7.7	7.4
EC (µS/m)	1405	1215	1023	273	387
pH_{zpc}	9	8.5	8.8	6.0	5.8
surface area (m^2/g)	231	66	27	195	28
Micropore vol (cm^3/g)	0.081	0.017	-	0.085	0.011
Ash (%)	43.2	38.5	28.2	35.7	32.9

Total Cd (mg/kg)	0.07	0.06	0.06	0.05	0.05

BM450 and BM600 (biochars prepared at 450 and 600 °C and modified by $MgCl_2$), BK450 (biochars prepared at 450 °C and modified by KOH), and B600, B450 (unmodified biochars prepared at 450 and 600°)

Results of pHzpc (Table 2) showed that pHzpc values of B600 and B450 were in acidic range, whereas pHzpc values of BM450, BM600 and BK450 were in the basic range, indicating that basic functional groups are predominant in the modified biochars surfaces, as stated by Nguyen et al. (2022) for a zinc-modified biochar and by Deng et al. (2021) for magnesium-modified biochars.

As expected (Shen et al., 2019), the results showed that the surface area and volume of the micropores increased with increasing pyrolysis temperature (Table 2). Also Shi et al. (2019) reported similar results on rice husk biochar, whose surface area increased from 0.63 to 193.1 m^2/g increasing the pyrolysis temperature from 300 to 700°C. In the same paper, they reported that biochar modification had a significant effect on the surface area. Also Chen et al. (2014) noted that by modification of biochar, the specific surface area increased from 25.4 to 67.6 m^2/g. In the case of our samples, no significant differences were observed with KOH modification at 450 °C, while modification with magnesium chloride increased the surface area of biochars either produced at temperature 450°C, which increased from 28 to 66 m^2/g, or at temperature 600°C, which increased from 195 to 231 m^2/g (Table 2). Only a small effect of $MgCl_2$ modification is visible on the microporosity of the systems.

FTIR analysis of modified and unmodified biochars is depicted in Fig. 1. An intense and large signal related to the stretching of O-H groups interacting via H bonding was present in the spectra of all biochar at 3400 cm^{-1} (Quan et al., 2020), whereas a narrow signal centered at 3700 cm^{-1}, due to isolated Si-OH functional groups, is present only in the spectra of the modified biochars, indicating the modification increases the number of OH groups and consequently the hydrophilicity of the biochars. Analogously, Deng et al. (2021) reported that a new strong adsorption peak was observed in 3469 cm^{-1} in magnesium-modified corn biochar, attributed to $Mg(OH)_2$ formation at the surface of the biochar. In the BK450 and BM600 biochars, three peaks were clearly observed below 3000 cm^{-1}, indicating the presence of aliphatic carbon chains

(stretching of C-H moieties). Additionally, carbonate-like groups (deriving from atmospheric CO_2 interaction with the basic surface of biochars) and physisorbed water molecules were evidenced in the spectra in the range of 1800 to 1200 cm^{-1}. Intense bands are present for carboxyl, ketone, C = C, and C = O groups at 1428, 1580 cm^{-1}, and 1099 cm^{-1}, respectively (Teng et al., 2020). Also, the Si-O-Si spectroscopic feature was observed at 1000 cm^{-1} in all biochars (Fig. 1), slightly shifted by modification procedure, which can be attributed to the presence of inorganic silica in the rice husk (Usman et al., 2016; Xiao et al., 2017). In all cases, it seems that modification introduced polar functionalities containing oxygen at the surface of biochars.

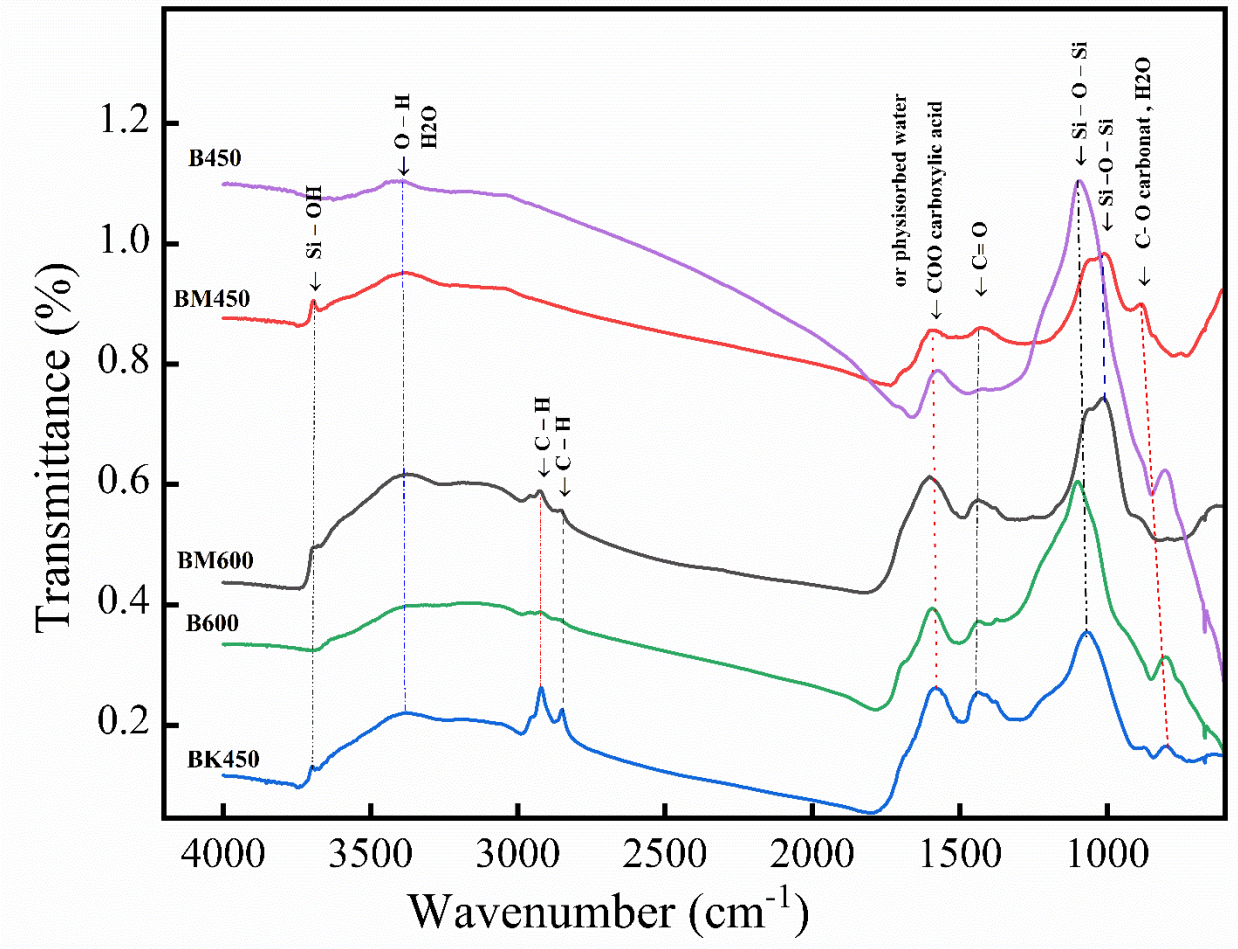

Fig. 1. FTIR analysis of unmodified biochars (BM450 and BM600), modified biochars (BK450, B600, and B450). The spectra were shifted to facilitate the observation of the curves.

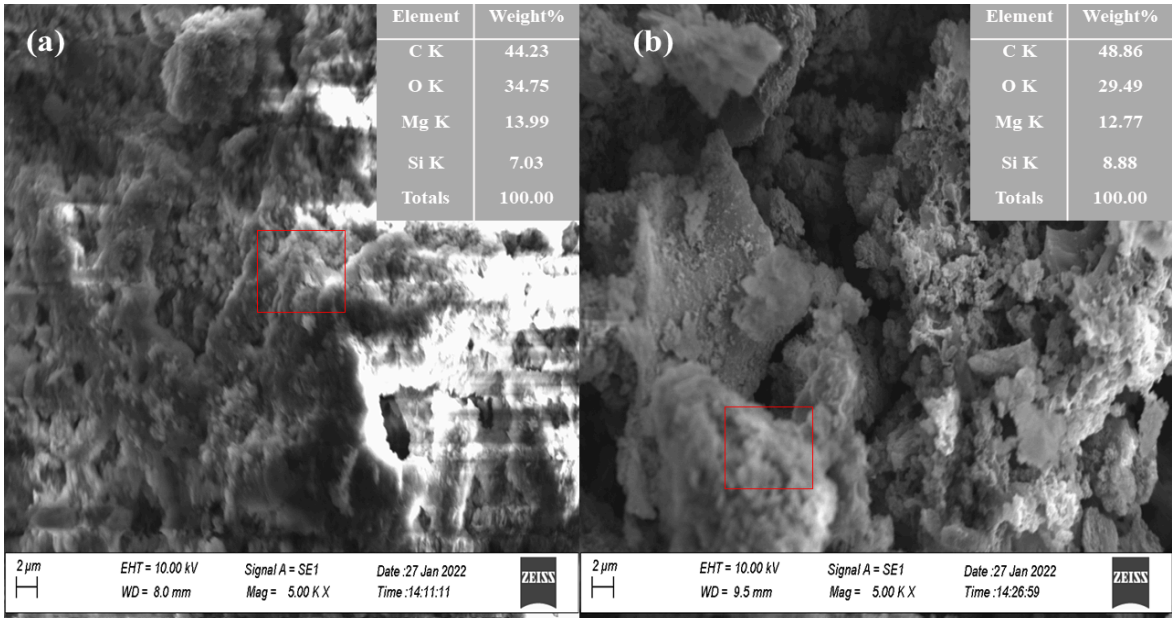
(a)
Element
Weight%
C K
44.23
O K
34.75
Mg K
13.99
Si K
7.03
Totals
100.00
2 µm
EHT = 10.00 kV
WD = 8.0 mm
Signal A = SE1
Mag = 5.00 K X
Date :27 Jan 2022
Time :14:11:11
ZEISS
(b)
Element
Weight%
C K
48.86
O K
29.49
Mg K
12.77
Si K
8.88
Totals
100.00
2 µm
EHT = 10.00 kV
WD = 9.5 mm
Signal A = SE1
Mag = 5.00 K X
Date :27 Jan 2022
Time :14:26:59
ZEISS

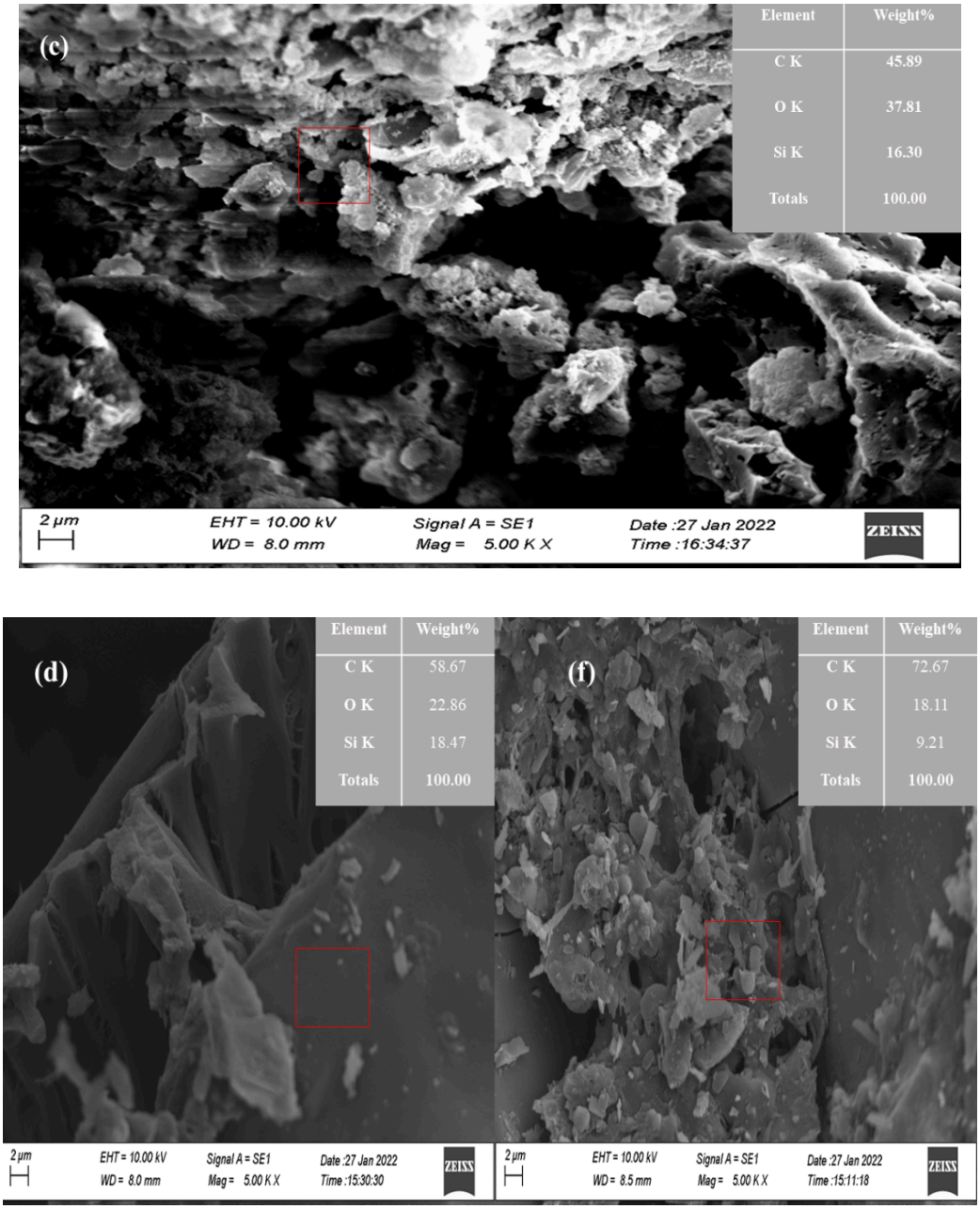

Fig. 2. SEM image - EDS of (a) BM450, (b) BM600(c), and BK450 (modified biochars), (d) B600, and (f) B450 (unmodified biochars).

SEM images (Fig. 2) showed structures similar to plant tissues in the B600 and B450 biochars surfaces. The increasing pyrolysis temperature from 450 to 600°C increased the irregularity of surfaces and introduce some macroporosity in the structure.

Irregular shapes and rough surfaces were also observed in BM450, BM600, and BM450. As biochar modification increased the irregularity and porosity of the structures. The surface morphology of BM450 exhibits a smoother aspect than BM600 and BK450. Also, the porosity and the extension of pores in the BM600 were higher than in BM450 (Figs. 2a and 2b).

The results of the EDS analyses confirmed the presence of a high magnesium content (>12%), probably present in the form of MgO as stated in (Yin et al., 2021), on the magnesium-modified biochar surfaces (Fig. 2), As a consequence of the successful loading of Mg on the biochar (Yin et al., 2018). On the contrary, potassium was not found on the biochar surface after the KOH modification process, and this could explain the similar results in terms of specific surface area and microporosity obtained from the samples B450 and BK450. The ratios O/C calculated using the EDS results for the modified samples BM600, BM450, BK450 were 0.60, 0.78, and 0.82, quite different and generally higher than the values obtained from the elemental analysis (0.48, 0.49, and 0.37, respectively), evidencing an increase of the oxygen content in the modified samples (as also observed by Akram et al. (2022), and confirming the FTIR results, whose evidenced the formation of oxygen-containing functionalities after biochar modification. In addition, as the EDS signals are related to the surface of the particles, while elemental analysis reflect the whole material, the increase of the oxygen content probably involves more the outermost layer of the material than its bulk.

3.2 Adsorption kinetics

Results of Cd adsorption kinetics on unmodified biochars (Fig. 3a) and modified biochars (Fig. 4a) showed a rapid adsorption in less than 1 h, followed by a slower adsorption up to 24 h. The adsorption reaction in the modified and unmodified biochars reached the equilibrium after 24 and 48 h, respectively. As reported in the literature (Xiao et al., 2017), this trend should be due to a rapid step controlled by the physisorption process followed by a slower step related to chemisorption process.

The highest adsorbed amount at the equilibrium was observed for BM600S (Fig. 4b). The values for the presoaked modified biochars were 98.4, 97.6, and 89.8 mg/g for BMS600, BMS450, and

BKS450, respectively, much more than the presoaked original biochars, showing 7.6 and 7.5 mg/g for B450 and B600, respectively (Fig. 3b). Adsorption equilibrium in presoaked modified biochars was 12 -14 times greater than that of unmodified ones. Also, in all biochars, Cd adsorption in presoaked materials was significantly larger ($p<0.05$) than in non-presoaked ones (Figs. 3b and 4b). This could have been due to a more efficient adsorptive/adsorbent contact in presoaked biochars, where the hydrophobicity of the samples (Gray et al., 2014) is at least partially mitigated.

Table 3

Data of kinetic model fitting for Cd adsorption in modified and unmodified rice husk biochars

Biochar type	**soaking status**	**Pseudo first order**			**Pseudo second order**			**Intraparticle diffusion**		
		q_e (mg/g)	k_1 (1/h)	R^2	q_e (mg/g)	k_2 (g/mgh)	R^2	q_e (mg/g)	K_d (mg/g $h^{0.5}$)	R^2
BM450	NS	94.01	0.235	0.99	94.82	0.01	0.99	108.5	9.39	0.77
	S	97.7	0.252	0.98	97.16	0.01	0.99	109.6	7.66	0.73
BM600	NS	94.35	0.184	0.98	95.35	0.101	0.99	111.6	11.42	0.78
	S	98.45	0.196	0.98	98.42	0.009	0.99	113.4	10.75	0.76
BK450	NS	85.05	0.235	0.89	84.71	0.011	0.99	96.99	9.59	0.88
	S	90.15	0.152	0.97	89.8	0.011	0.99	101.2	8.87	0.83
B600	NS	7.11	0.167	0.91	7.11	0.135	0.99	7.95	0.729	0.91
	S	7.52	0.182	0.99	7.52	0.131	0.99	8.34	0.555	0.77
B450	NS	7.37	0.115	0.98	7.289	0.132	0.99	8.09	0.71	0.91
	S	7.56	0.171	0.99	7.65	0.129	0.99	8.51	0.577	0.75

Pseudo-first order, Pseudo-second order, and Intraparticle diffusion models were used to model Cd adsorption kinetic (Table 3). Among the three models, the Pseudo-second order model showed the highest correlation coefficient ($R^2 > 0.99$) and well simulated the results of the Cd adsorption process in modified and unmodified biochars. The adsorption equilibrium values obtained from the Pseudo-second order model were very close to the experimental results, revealing that the chemisorption in the form of cation exchange, precipitation, and inner-sphere

complexes, is likely the main process controlling Cd adsorption on the biochar (Usman et al., 2016). These mechanisms were also described by Liu and Fan (2018), who noted that the precipitation with minerals was the main process in the removal of Cd by wheat straw biochar, and also the surface complex process played an important role. In a similar study, Lou et al. (2012) reported that the chemisorption of Pb on biochar was in the form of inner-sphere complexes, exchange with Ca and Mg ions, and complexation with surface functional groups. Also, the Pseudo-first order model well fitted ($R^2 > 0.91$) the kinetic data, indicating that also mass transfer is one of the important processes in the adsorption of Cd on the biochar surface. On the base of all these results, it can be suggested that chemisorption and mass transfer mainly control Cd removal mechanism.

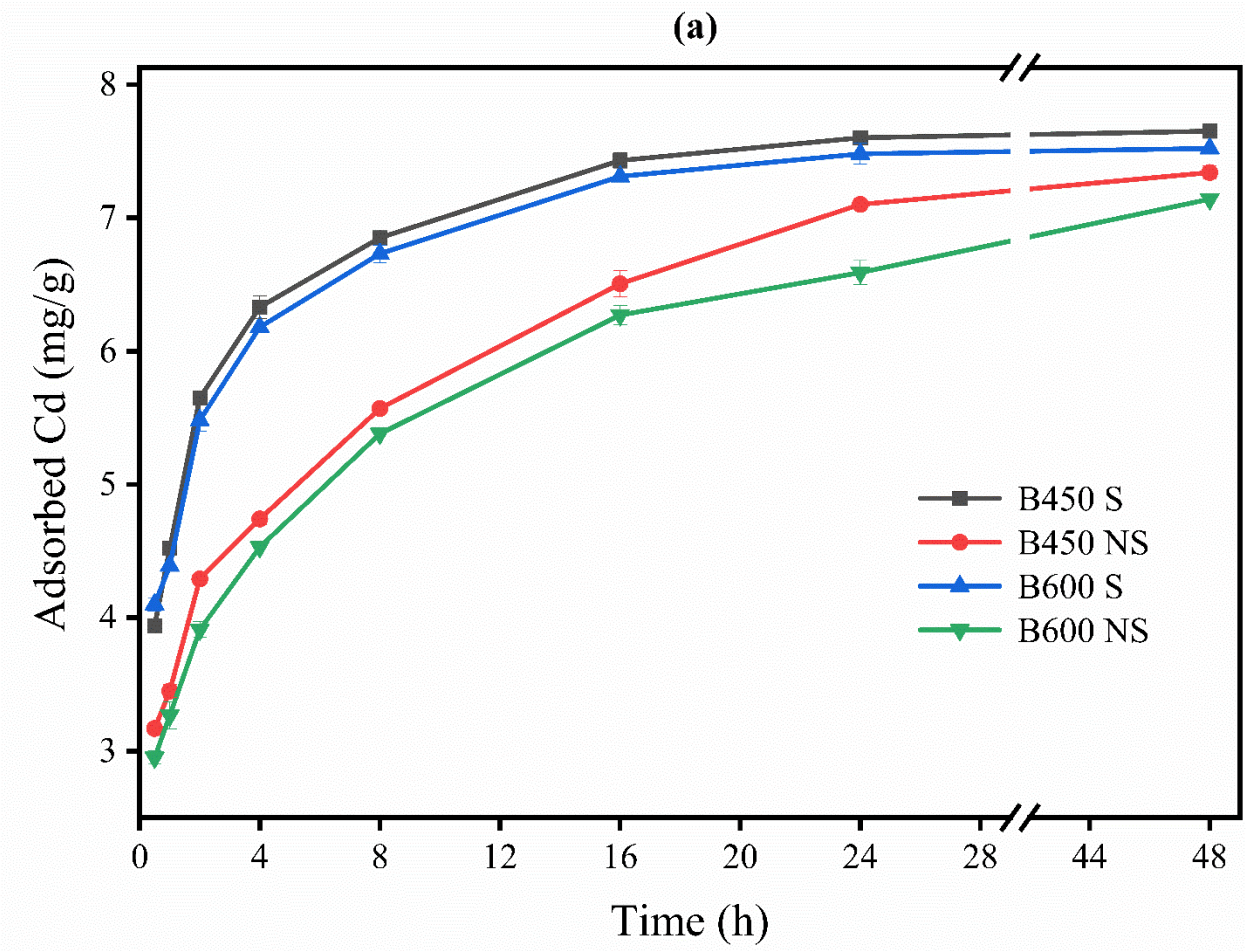
(a)
Adsorbed Cd (mg/g)
Time (h)
B450 S
B450 NS
B600 S
B600 NS
8
7
6
5
4
3
0
4
8
12
16
20
24
28
44
48

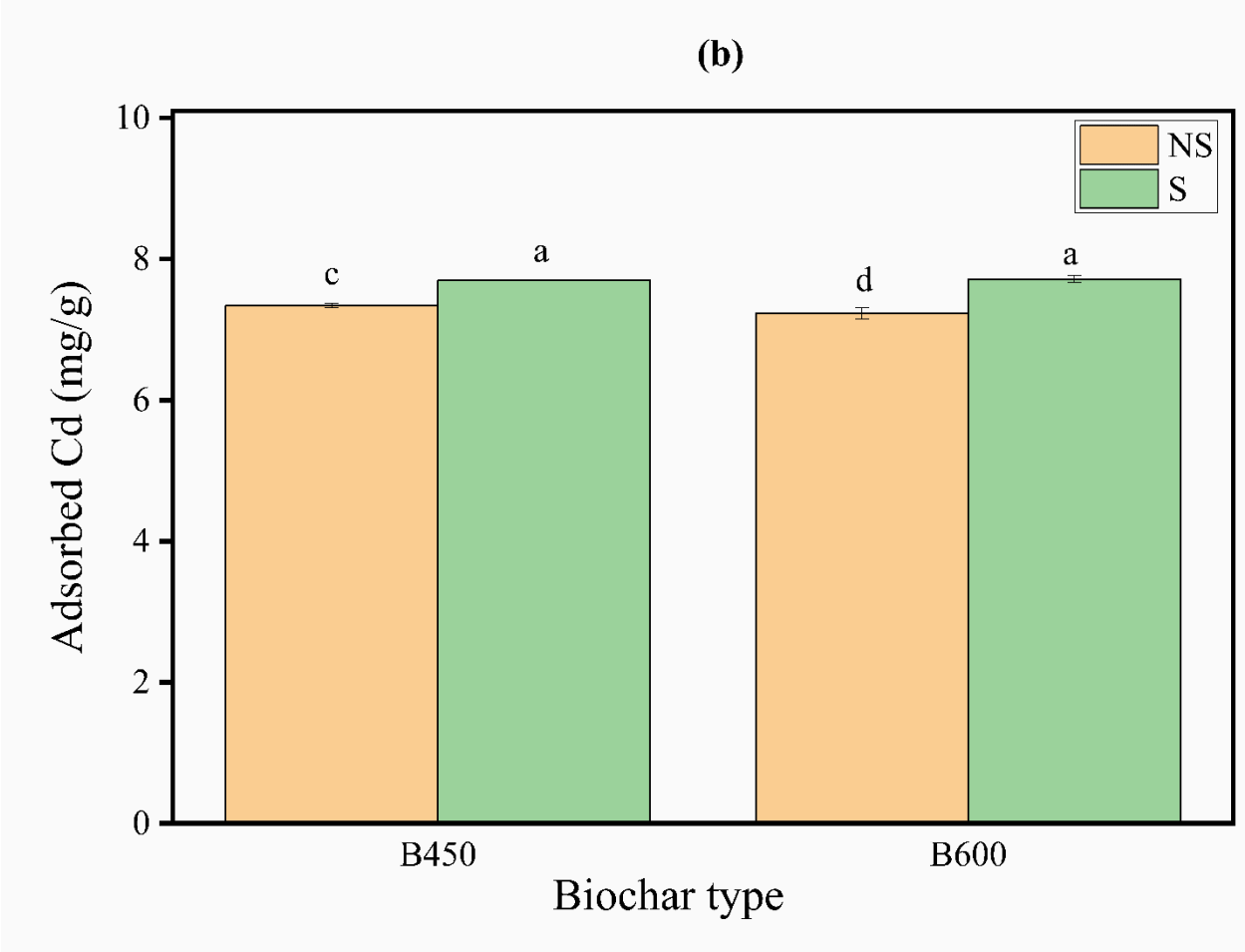

Fig. 3. (a) Adsorption kinetics of Cd in (S) presoaked and (NS) non-presoaked B450 and B600, and (b) Equilibrium Cd adsorption in (S) presoaked and (NS) non-presoaked B450 and B600, letters a, b, c and d indicate a significant difference ($p < 0.05$) among treatments by Duncan test.

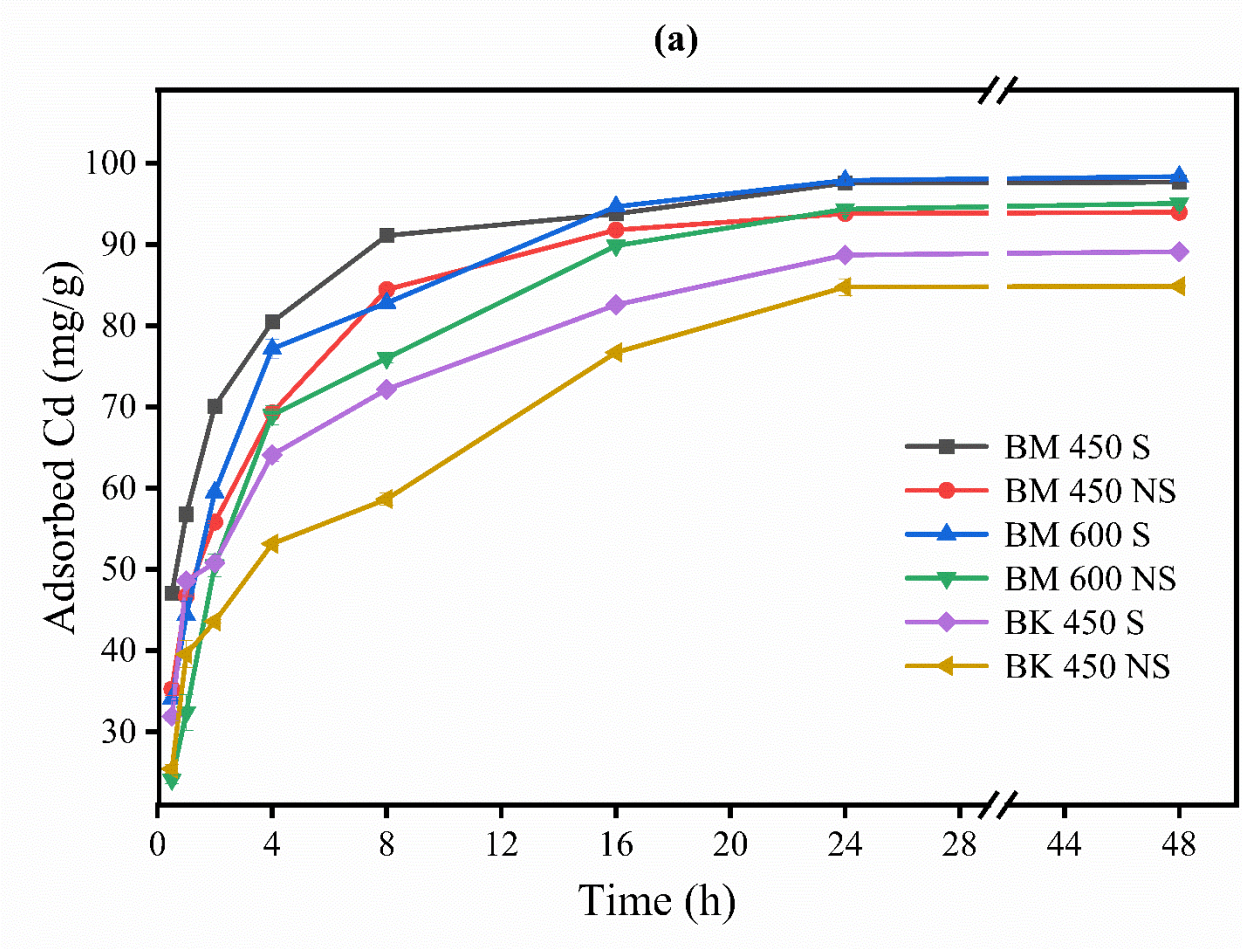
(a)
Adsorbed Cd (mg/g)
100
90
80
70
60
50
40
30
0
4
8
12
16
20
24
28
44
48
Time (h)
BM 450 S
BM 450 NS
BM 600 S
BM 600 NS
BK 450 S
BK 450 NS

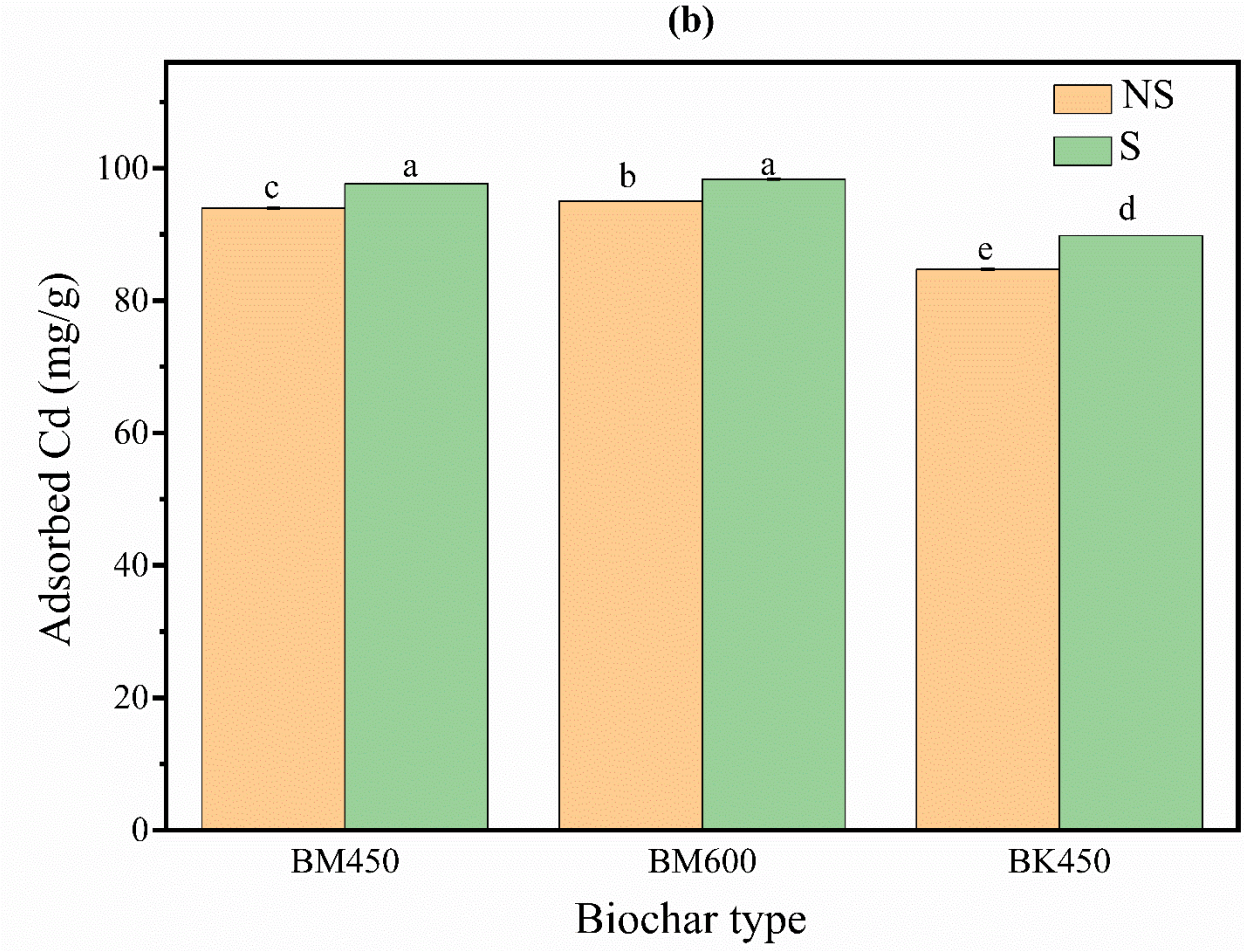

Fig. 4. (a) Adsorption kinetics of Cd in (S) presoaked and (NS) non-presoaked BM600, BM450, and BK450 , and (b) Equilibrium Cd adsorption in the presoaked(s) and (NS) non-presoaked BM600, BM450, and BK450, letters a, b, c, d, e, and f indicate a significant difference ($p < 0.05$) among treatments by Duncan test.

3.3 Effect of experimental conditions applied to biochar presoaking process

In the following paragraph the effect of material particle size, adsorption temperature and solution pH were investigated in order to achieve the best conditions necessary for an efficient removal of Cd. Only the non-modified samples were examined, with the idea that all the conclusions achieved for them could be transferred to the modified samples with even better results.

A) Effect of particle size

Considering the different sizes of biochar particles, the total amount of adsorbed Cd was significantly higher for the biochar grinded at 100 µm than one at 500 µm. The results showed that Cd adsorption was higher in presoaked biochars (either B600 or B450) than in non-presoaked biochars, regardless of the reaction time (Figs. 5a and 5b). The presoaking effect was more important for the coarser particles (500 µm). Also considering the adsorption kinetics the biochar size played a role. The time to reach the equilibrium was reduced from 48 to 24 h with presoaking and decreasing biochar particle size. The increased adsorption and reduced equilibrium time was presumably partly due to the creation of new pores and to the increase of the specific surface area in smaller particles. Smaller particles are also more conductive and have higher densities of functional groups at the external pores (Jin et al., 2022), which can increase the biochar reactivity and the amount of adsorption. Another possible mechanism increasing the adsorption of smaller particle sizes is the formation of graphite-like structures and nanostructures (Song et al., 2019). Jin et al. (2022), reported a positive correlation between biochar size and graphite structures and functional groups.

Smaller biochars particles had more Graphite-like structures and functional groups, therefore they were more active and had a higher adsorption rate than biochars with larger sizes. In a similar study, Hameed and lin. (2020) showed that the amount of adsorption of phenanthrene, atrazine, and oxytetracycline was higher in biochars with smaller size particles that were produced at higher pyrolysis temperatures. They noted increased adsorption due to the formation of graphitic domains, structural defects, presence of aromatic carbon and increased surface area. In conclusion, it seems that small particle size(typical of high surface area samples), formation of graphitic domains and structural defects increase adsorption capacity.

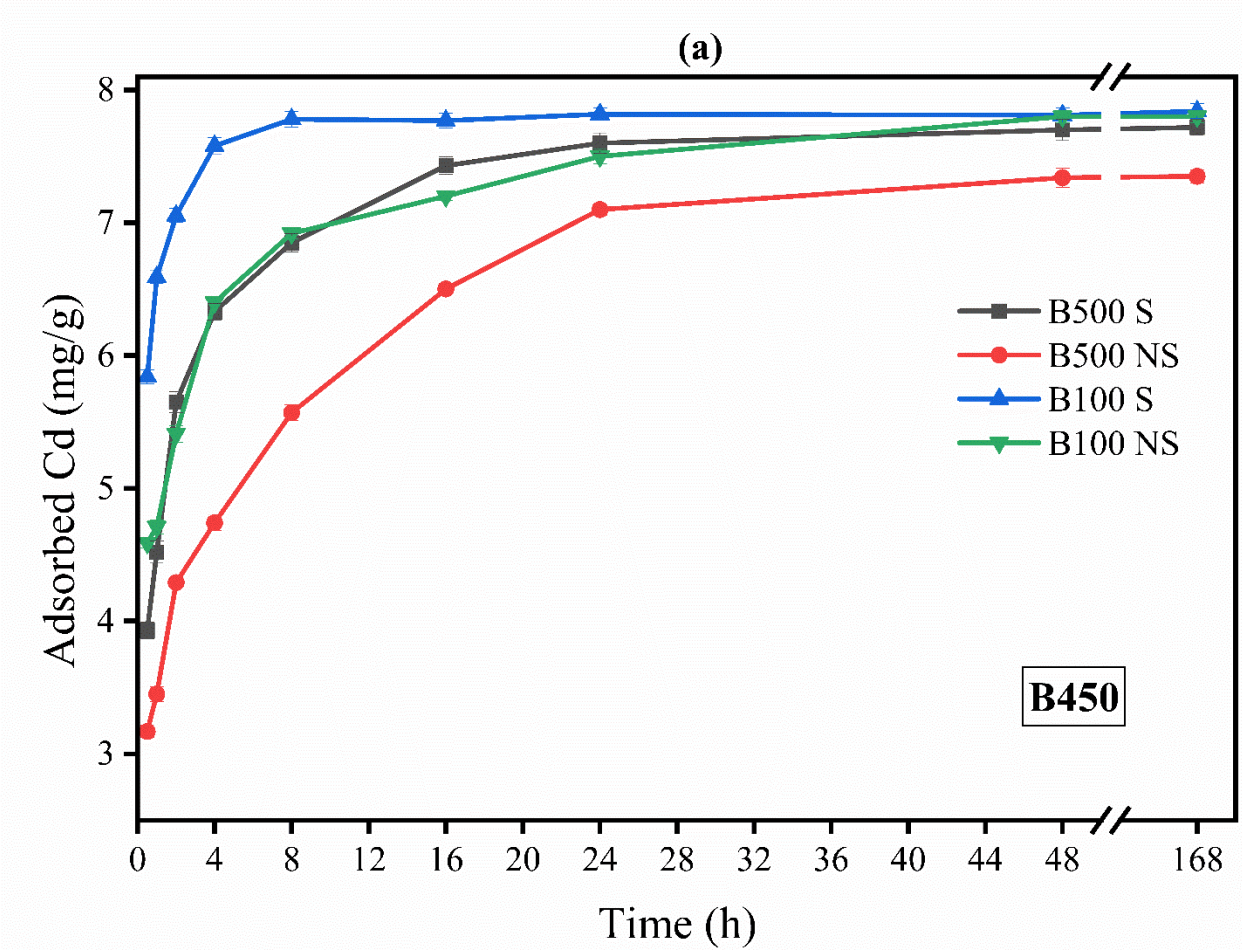
(a)
Adsorbed Cd (mg/g)
Time (h)
B500 S
B500 NS
B100 S
B100 NS
B450
0
4
8
12
16
20
24
28
32
36
40
44
48
168
3
4
5
6
7
8

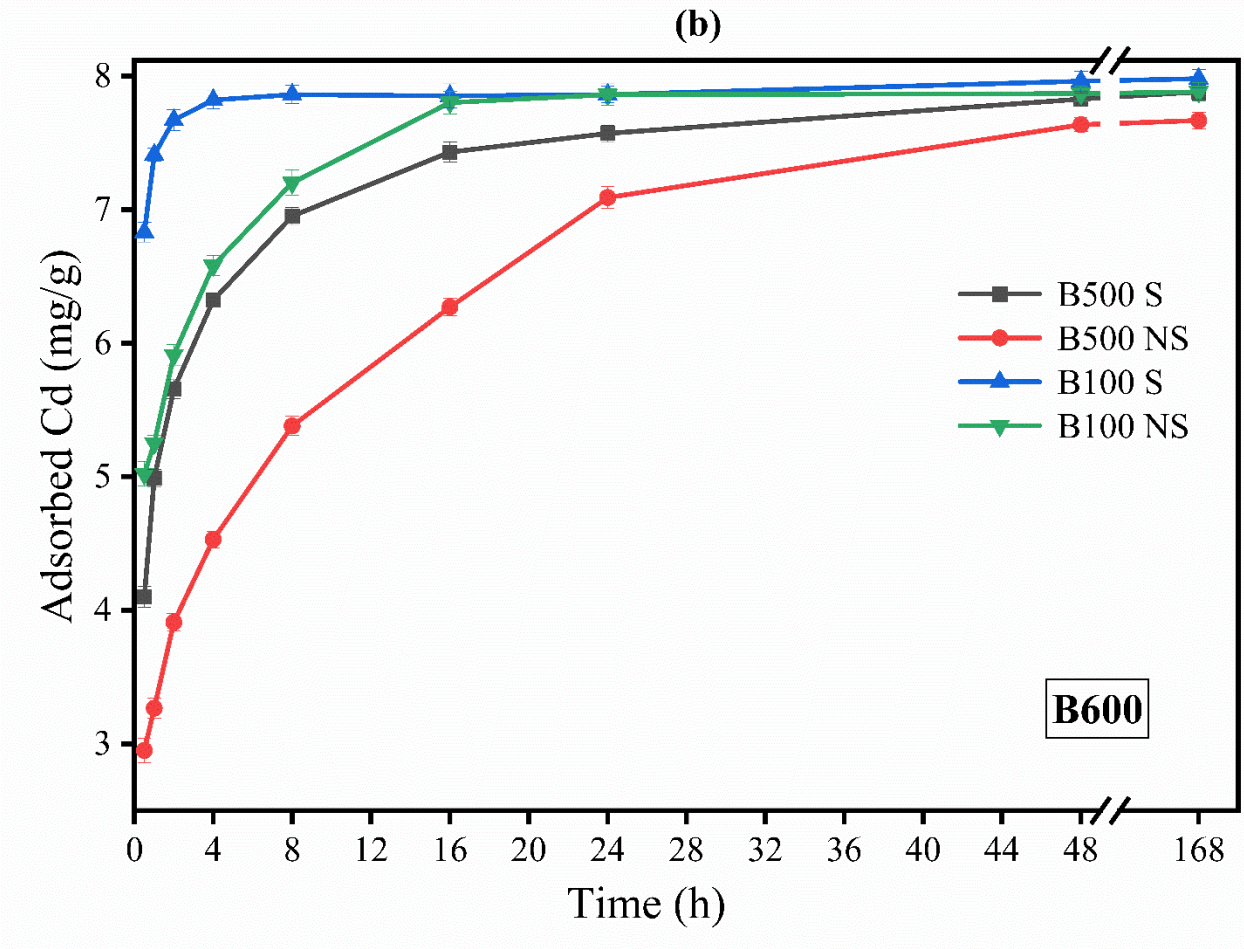

Fig. 5. Effect of biochar particle size on Cd adsorption kinetics in (S) presoaked and (NS) non-presoaked unmodified biochars grinded at 500 and 100µm size.

B) Effect of adsorption temperature

T The effect of presoaking on the Cd adsorption kinetics on B450 and B600 biochars at different temperatures is shown in Figs. 6a and 6b. The highest adsorption was observed in the presoaked biochars at 35 °C and the lowest adsorption was observed in the non-presoaked biochars at 15 °C. At all temperatures, presoaked biochars adsorbed significantly more than non-presoaked biochars, and the effect of presoaking decreased at increasing contact times. Also, the time to reach the equilibrium decreased with presoaking and increasing temperatures, from 48 h at 15 °C to 24 h at 35 °C. In the earlier contact times, increasing temperatures from 15 to 35 °C significantly increased Cd adsorption in presoaked biochars than in non-presoaked.

Also, increasing the temperature reduced the density of the suspension, which increases the rate of solute diffusion to the external and internal pores, affecting the adsorption and decreasing the time to reach the equilibrium.

In general, two driving forces are involved in the adsorption process; enthalpy (ΔH) and entropy (ΔS) of reaction (Brown et al., 1969). Previous studies reported that the enthalpy of the Cd adsorption process is small and positive, indicating that the adsorption is endothermic (Deng et al., 2012). It has been reported that also the entropy of the Cd adsorption is positive, due to the increase in randomness at the interface between particles and the solution (Wang et al., 2017). At the expense of ΔS and ΔH, the ΔG is a negative value. Xiang et al. (2018) measured ΔG values for the Cd adsorption at temperatures of 25, 35 and 45°C of -8,612, -8,901, and 9.191 KJ/mol, respectively. Therefore, the Cd adsorption process is a non-spontaneous and endothermic reaction, so Cd adsorption should increase at increasing temperatures (Taha et al., 2016; Zhao et al., 2014).

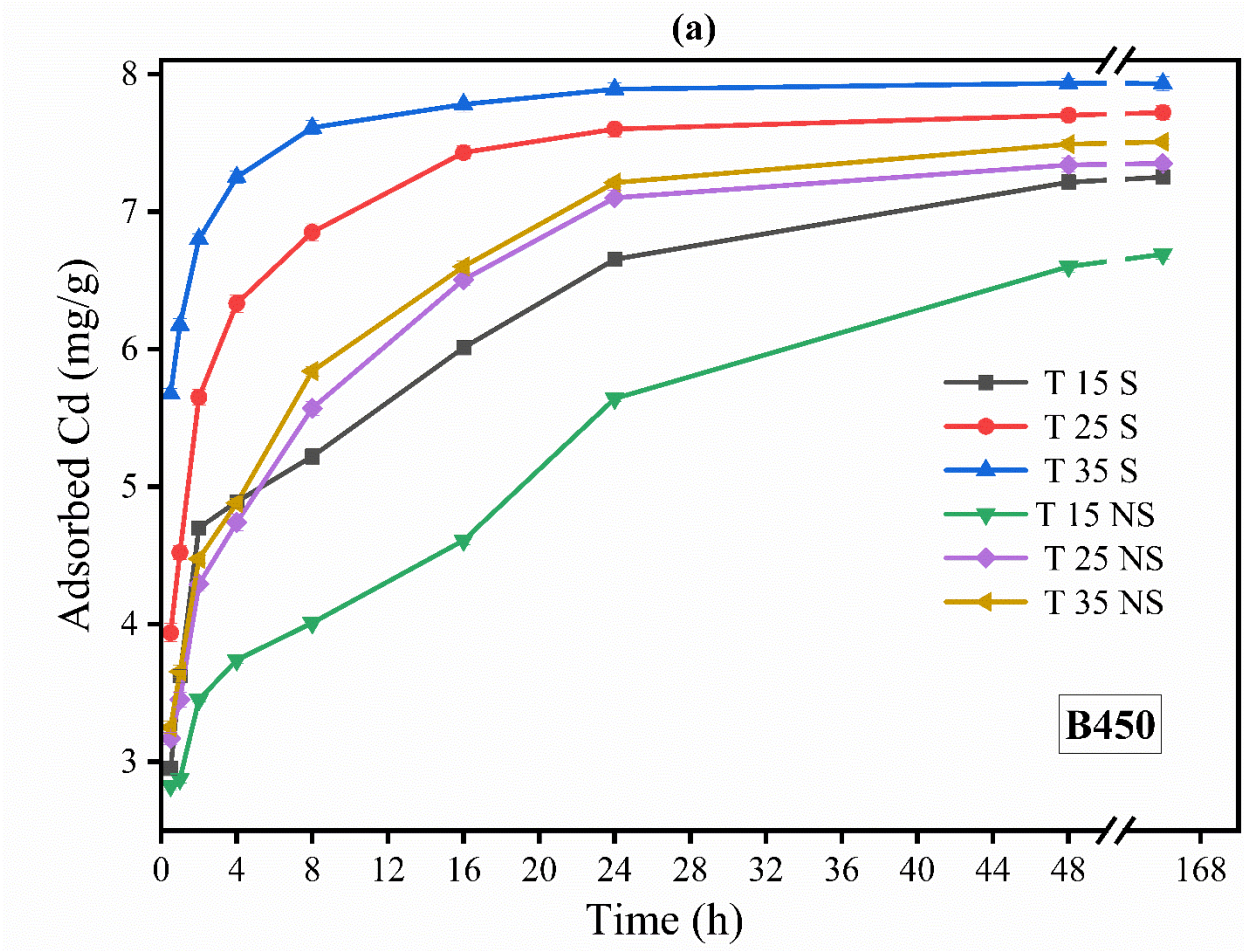
(a)
Adsorbed Cd (mg/g)
Time (h)
T 15 S
T 25 S
T 35 S
T 15 NS
T 25 NS
T 35 NS
B450

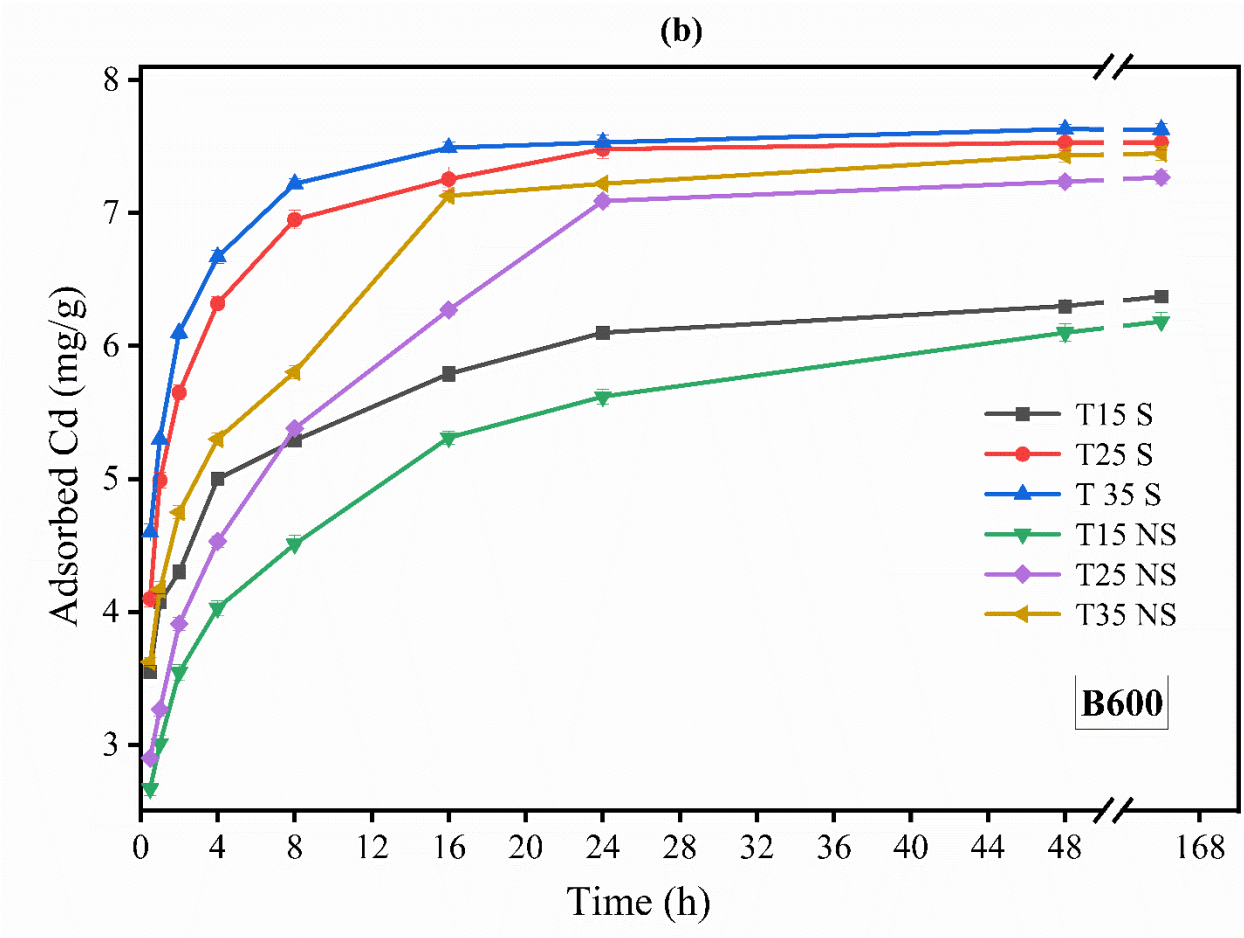

Fig. 6. Effect of temperature on Cd adsorption kinetics in (S) presoaked and (NS) non-presoaked. T15S, T25S, and T35S are presoaked biochars at 15, 25, and 35 °C, respectively. T15NS, T25NS, and T35NS are non-presoaked biochars at 15, 25, and 35 °C, respectively.

C) Effect of pH

In this study, the effect of biochar presoaking on Cd adsorption was examined at pHs 2, 5 and 6, as tested in previous studies (Sun et al., 2019; Qiu et al., 2019). The results are reported in Figs. 7a and 7b. The highest Cd adsorption was observed in presoaked biochars at pH 6 and the lowest adsorption was observed in the pristine biochars at pH 2. Cd adsorption values for B450 and B600 biochars at all contact times were significantly higher in presoaked biochars than in non-presoaked. The adsorption significantly increased, also increasing the pH from 2 to 6, which

can be related to pH_{pzc} of biochars. According to our analyses (Table 2), at the highest pH tested the pH was higher than the pH_{pzc} for the B450, while equal to the pH_{pzc} for the B600. As the result, competition between protons and Cd ions on the biochar surface was lower and Cd adsorption was greater.

Previous studies showed that changes in pH affected both the properties of the adsorbent and the adsorbate. The main effect of pH on biochar surface is the protonation and the deprotonation of functional groups such as carboxyls, hydroxyls and phenols. Increasing the pH will increase the Cd adsorption for the deprotonation of functional groups, which increases the negative charge density at the biochar surfaces, and for the decreased competition between protons and Cd ions at adsorption sites (Usman et al., 2016). On the other hand, pH is also an important parameter affecting ion speciation and, thus, ion adsorption (Wen et al., 2022). Wang et al. (2022), for example, observed that the adsorption of antibiotics on biochar decreased with decreasing pH due to the protonation of the functional groups and the creation of a positive charge.

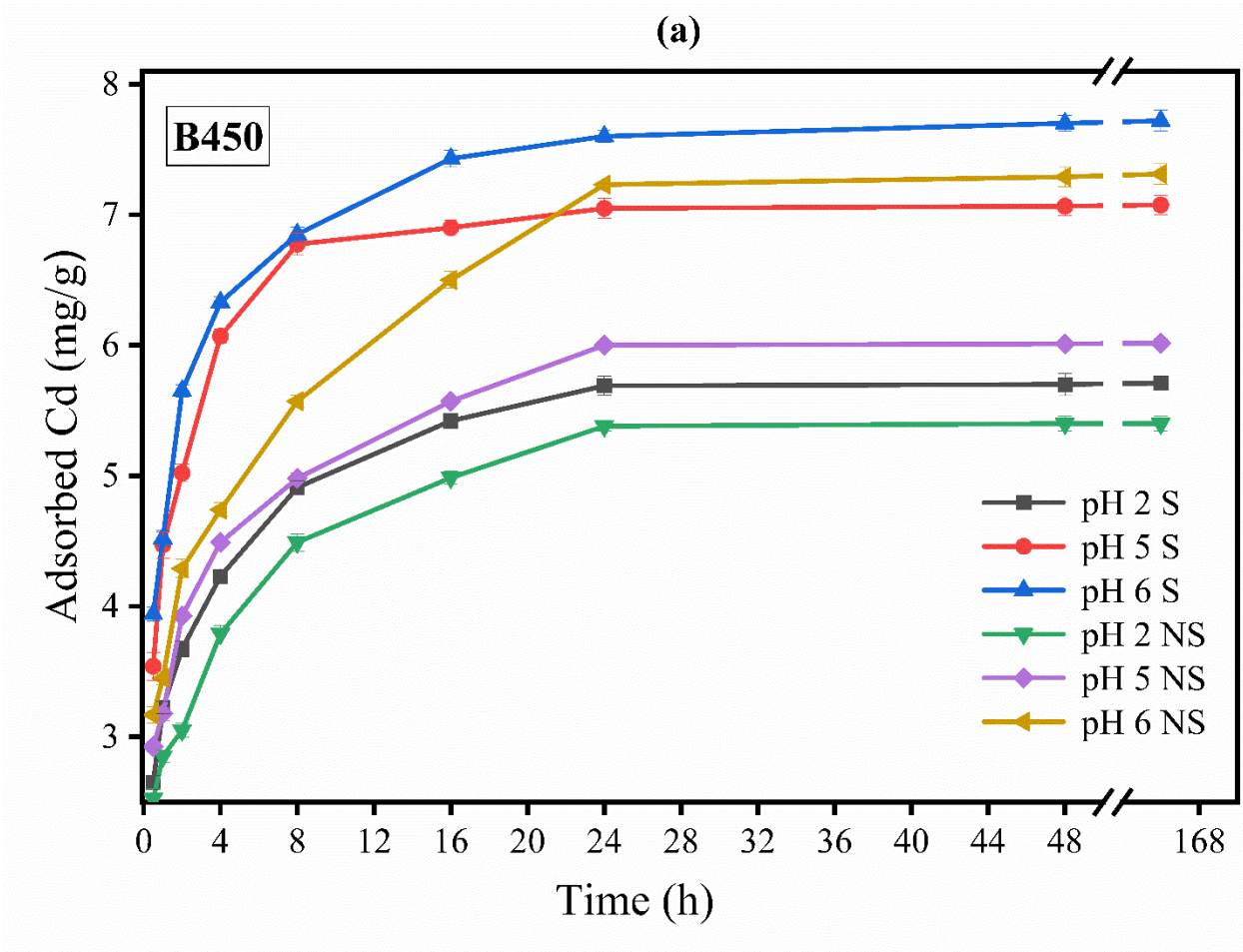
(a)
B450
Adsorbed Cd (mg/g)
Time (h)
pH 2 S
pH 5 S
pH 6 S
pH 2 NS
pH 5 NS
pH 6 NS
0
4
8
12
16
20
24
28
32
36
40
44
48
168
3
4
5
6
7
8

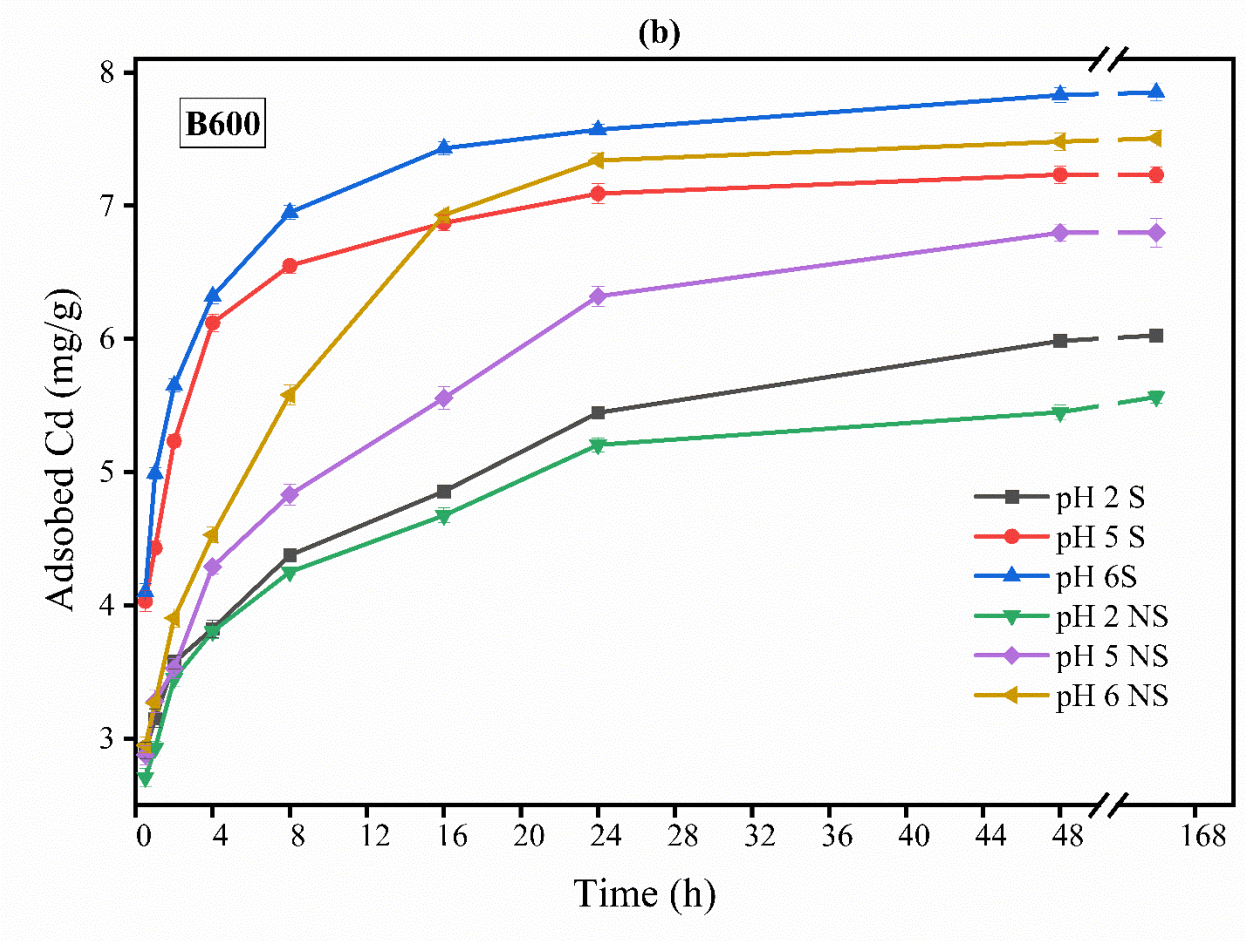

Fig. 7. Effect of pH on Cd adsorption kinetics in (S) presoaked and (NS) non-presoaked unmodified biochars

4. Conclusions

The difference in cadmium adsorption between presoaked and non-presoaked biochars over a range of pH, temperature, and biochar particle size showed that presoaking had a significant effect on Cd adsorption on rice husk biochar on both original and the modified biochars. The modified biochars had a higher adsorption capacity, and thus differences between presoaked and non-presoaked materials were greater than in unmodified biochars.

The presoaking step increased the contact of biochar with the external solution, as evidenced from the lower time needed to reach the equilibrium for presoaked biochars and from the decrease of these differences at increasing contact times. The presoaking effect was more

evident at lower temperatures and with coarser biochar particles, while decreasing the particle size and increasing the temperature the effect of soaking decreased. However, increasing the temperature requires energy, and it is also more difficult to separate smaller biochars from aqueous media. As a result, biochar soaking before use seems to be an effective way to increase the adsorption and to reduce the time to reach the equilibrium, making more efficient the adsorption process.

Acknowledgments

The authors would like to appreciate the Department of Soil Science at the University of Tehran for funding this project. The authors also thank the technical staff Agricultural Chemistry and pedology unit in the Department of agronomy and food science of the University of Turin, Italy for providing the instrumentation required for biochar and cadmium analysis and also the staff of the Agricultural Chemistry and pedology unit of the University of Turin (Italy) for their help and support.

References

Abdel-Halim, E. S., & Al-Deyab, S. S., 2011. Removal of heavy metals from their aqueous solutions through adsorption onto natural polymers. Carbohydrate Polymers, 84(1), 454-458.

Akram, A., Muzammal, S., Shakoor, M. B., Ahmad, S. R., Jilani, A., Iqbal, J., Kalam, A., & Aboushoushah, S. F. O. 2022. Synthesis and Application of Egg Shell Biochar for As (V) Removal from Aqueous Solutions. J. Catalysts, 12(4), 431.

Berslin, D., Reshmi, A., Sivaprakash, B., Rajamohan, N., & Kumar, P. S., 2021. Remediation of emerging metal pollutants using environment-friendly biochar-Review on applications and mechanism. Chemosphere, 133384.

Brown, T. L., LeMay, H. E., Bursten, B. E., Murphy, C. J., & Woodward, P. M., 1969. J. Chemistry: the central science (Vol. 12). Prentice-Hall.

Chen, T., Zhang, Y., Wang, H., Lu, W., Zhou, Z., Zhang, Y., & Ren, L., 2014. Influence of pyrolysis temperature on characteristics and heavy metal adsorptive performance of biochar derived from municipal sewage sludge. J. Bioresource technology, 164, 47-54.

Cheng, Q., Huang, Q., Khan, S., Liu, Y., Liao, Z., Li, G., & Ok, Y. S., 2016 . Adsorption of Cd by peanut husks and peanut husk biochar from aqueous solutions. J. Ecological Engineering, 87, 240-245.

Coles, C. A., & Yong, R. N., 2002. Aspects of kaolinite characterization and retention of Pb and Cd. J. Applied Clay Science, 22(1-2), 39-45.

Corapcioglu, M. O., & Huang, C. P., 1987. The adsorption of heavy metals onto hydrous activated carbon. J. Water research, *21*(9), 1031-1044.

Deng, J., Liu, Y., Liu, S., Zeng, G., Tan, X., Huang, B., & Yan, Z., 2017. Competitive adsorption of Pb (II), Cd (II,), and Cu (II) onto chitosan-pyromellitic dianhydride modified biochar. J. Colloid and Interface Science, 506, 355-364.

Deng, Y., Li, X., Ni, F., Liu, Q., Yang, Y., Wang, M., Ao, T., & & Chen, W., 2021. Synthesis of magnesium modified biochar for removing copper, lead, and cadmium in single and binary systems from aqueous solutions: Adsorption Mechanism. J. Water, 13(5), 599.

Faria, P. C. C., Orfao, J. J. M., & Pereira, M. F. R., 2004. Adsorption of anionic and cationic dyes on activated carbons with different surface chemistries. J. Water Research, 38(8), 2043-2052.

Gray, M., Johnson, M. G., Dragila, M. I., & Kleber, M., 2014. Water uptake in biochars: the roles of porosity and hydrophobicity. J. Biomass and Bioenergy, 61, 196-205.

Hameed, R., Lei, C., & Lin, D., 2020. Adsorption of organic contaminants on biochar colloids: effects of pyrolysis temperature and particle size .J. Environmental Science and Pollution Research, 27(15), 18412-18422.

Ho, Y. S., & McKay, G., 1999. Pseudo-second order model for sorption processes. J. Process Biochemistry, 34(5), 451-465.

Huang, F., Zhang, S. M., Wu, R. R., Zhang, L., Wang, P., & Xiao, R. B., 2021. Magnetic biochars have lower adsorption but higher separation effectiveness for Cd^{2+} from aqueous solution compared to nonmagnetic biochars. J. Environmental Pollution, 275, 116485.

Ighalo, J. O., Adeniyi, A. G., Eletta, O. A., & Arowoyele, L. T., 2020. Competitive adsorption of Pb (II), Cu (II), Fe (II), and Zn (II) from aqueous media using biochar from oil palm (*Elaeis guineensis*) fibers: a kinetic and equilibrium study. J. Indian Chemical Engineer, 1-11.

Inyang, M., Gao, B., Yao, Y., Xue, Y., Zimmerman, A. R., Pullammanappallil, P., & Cao, X. (2012). Removal of heavy metals from aqueous solution by biochars derived from anaerobically digested biomass. *Bioresource technology*, *110*, 50-56.

Jin, Z., Xiao, S., Dong, H., Xiao, J., Tian, R., Chen, J., & Li, L., 2022. Adsorption and catalytic degradation of organic contaminants by biochar: Overlooked role of biochar's particle size. J. Hazardous Materials, 422, 126928.

Joseph, L., Jun, B. M., Flora, J. R., Park, C. M., & Yoon, Y., 2019. Removal of heavy metals from water sources in the developing world using low-cost materials J. A review. Chemosphere, 229, 142-159.

Kampalanonwat, P., & Supaphol, P., 2014. The study of competitive adsorption of heavy metal ions from aqueous solution by aminated polyacrylonitrile nanofiber mats. J. Energy Procedia, 56, 142-151.

Khoo, K. S., Chia, W. Y., Chew, K. W., & Show, P. L., 2021. Microalgal-bacterial consortia as a prospect in wastewater bioremediation, environmental management, and bioenergy production. Indian Journal of Microbiology, 1-8.

Kloss, S., Zehetner, F., Dellantonio, A., Hamid, R., Ottner, F., Liedtke, V., & Soja, G., 2012. Characterization of slow pyrolysis biochars: effects of feedstocks and pyrolysis temperature on biochar properties. J. Environmental Quality, 41(4), 990-1000.

Kumar, S., Islam, A. R. M. T., Islam, H. T., Hasanuzzaman, M., Ongoma, V., Khan, R., & Mallick, J., 2021. Water resources pollution associated with risks of heavy metals from Vatukoula Goldmine region, Fiji. J. Environmental Management, 293, 112868.

Lagergren, S., 1898. Zur theorie der sogenannten adsorption geloster stoffe. Kungliga svenska vetenskapsakademiens. Handlingar, 24, 1-39.

Li, X., Wang, C., Zhang, J., Liu, J., Liu, B., & Chen, G., 2020. Preparation and application of magnetic biochar in water treatment: A critical review. Science of the J. Total Environment, 711, 134847.

Liu, L., & Fan, S., 2018. Removal of cadmium in aqueous solution using wheat straw biochar: effect of minerals and mechanism. J. Environmental Science and Pollution Research, 25(9), 8688-8700.

Liu, X., Hicher, P., Muresan, B., Saiyouri, N., & Hicher, P. Y., 2016. Heavy metal retention properties of kaolin and bentonite in a wide range of concentrations and different pH conditions. J. Applied Clay Science, 119, 365-374.

Lu, H., Zhang, W., Yang, Y., Huang, X., Wang, S., & Qiu, R. (2012). Relative distribution of Pb2+ sorption mechanisms by sludge-derived biochar. Water research, 46(3), 854-862.

Monser, L., & Adhoum, N, 2002. Modified activated carbon for the removal of copper, zinc, chromium, and cyanide from wastewater. J. Separation and purification technology, 26(2-3), 137-146.

Nguyen, T. B., Truong, Q. M., Chen, C. W., Doong, R. A., Chen, W. H., & Dong, C. D., 2022. Mesoporous and adsorption behavior of algal biochar prepared via sequential hydrothermal carbonization and $ZnCl_2$ activation. J. Bioresource technology, 346, 126351.

Oh, S. Y., & Seo, Y. D., 2019. Factors affecting the sorption of halogenated phenols onto polymer/biomass-derived biochar: Effects of pH, hydrophobicity, and deprotonation. J. Environmental Management, 232, 145-152.

Oliveira, W. E., Franca, A. S., Oliveira, L. S., & Rocha, S. D., 2008. Untreated coffee husks as biosorbents for the removal of heavy metals from aqueous solutions. J. Hazardous Materials, 152(3), 1073-1081.

Park, C. M., Han, J., Chu, K. H., Al-Hamadani, Y. A., Her, N., Heo, J., & Yoon, Y., 2017. Influence of solution pH, ionic strength, and humic acid on cadmium adsorption onto activated biochar: experiment and modeling. J. Industrial and Engineering Chemistry, 48, 186-193.

Qiu, Y., Zhang, Q., Li, M., Fan, Z., Sang, W., Xie, C., & Niu, D., 2019. Adsorption of Cd (II) from aqueous solutions by modified biochars: comparison of modification methods. J. Water, Air, & Soil Pollution, 230(4), 1-11.

Quan, G., Fan, Q., Sun, J., Cui, L., Wang, H., Gao, B., & Yan, J., 2020. Characteristics of organo-mineral complexes in contaminated soils with long-term biochar application. J. hazardous materials, 384, 121265.

Rajendran, S., Priya, T. A. K., Khoo, K. S., Hoang, T. K., Ng, H. S., Munawaroh, H. S. H., Karaman, C., Orooji, y., & Show, P. L., 2022. A critical review on various remediation approaches for heavy metal contaminants removal from contaminated soils. J. Chemosphere, 287, 132369

Rego, F., Xiang, H., Yang, Y., Ordovás, J. L., Chong, K., Wang, J., & Bridgwater, A., 2022. Investigation of the role of feedstock properties and process conditions on the slow pyrolysis of biomass in a continuous auger reactor. J. Analytical and Applied Pyrolysis, 161, 105378.

Shakoor, M. B., Ali, S., Rizwan, M., Abbas, F., Bibi, I., Riaz, M., & Rinklebe, J., 2020. A review of biochar-based sorbents for the separation of heavy metals from water. International J. Phytoremediation, 22(2), 111-126.

Shen, Z., Hou, D., Jin, F., Shi, J., Fan, X., Tsang, D. C., & Alessi, D. S., 2019. Effect of production temperature on lead removal mechanisms by rice straw biochars. Science of the J. Total Environment, 655, 751-758.

Shi, J., Fan, X., Tsang, D. C., Wang, F., Shen, Z., Hou, D., & Alessi, D. S., 2019. Removal of lead by rice husk biochars produced at different temperatures and implications for their environmental utilizations. J. Chemosphere, 235, 825-831.

Singh, B., Camps-Arbestain, M., & Lehmann, J., 2017 . Biochar: a guide to analytical methods. Csiro Publishing.

Singh, E., Kumar, A., Mishra, R., You, S., Singh, L., Kumar, S., & Kumar, R., 2021. Pyrolysis of waste biomass and plastics for production of biochar and its use for removal of heavy metals from aqueous solution .J. Bioresource Technology, 320, 124278.

Song, B., Chen, M., Zhao, L., Qiu, H., & Cao, X., 2019. Physicochemical property and colloidal stability of micron-and nano-particle biochar derived from a variety of feedstock sources. J.J Science of the Total Environment, 661, 685-695.

Sun, C., Chen, T., Huang, Q., Wang, J., Lu, S., & Yan, J., 2019. Enhanced adsorption for Pb (II) and Cd (II) of magnetic rice husk biochar by KMnO4 modification .J. Environmental Science and Pollution Research, 26(9), 8902-8913.

Teng, D., Zhang, B., Xu, G., Wang, B., Mao, K., Wang, J., Feng, X., Yang, Z., & Zhang, H., 2020. Efficient removal of Cd (II) from aqueous solution by pinecone biochar: Sorption performance and governing mechanisms. Environnemental Pollution, 265, 115001.

Usman, A., Sallam, A., Zhang, M., Vithanage, M., Ahmad, M., Al-Farraj, A., & Al-Wabel, M., 2016. Sorption process of date palm biochar for aqueous Cd (II) removal: Efficiency and mechanisms. J. Water, Air, & Soil Pollution, 227(12), 1-16.

Wang, H., Wang, X., Ma, J., Xia, P., & Zhao, J., 2017. Removal of cadmium (II) from aqueous solution: a comparative study of raw attapulgite clay and a reusable waste–struvite/attapulgite obtained from nutrient-rich wastewater. J. Hazardous Materials, 329, 66-76.

Wang, J., Zheng, S., Shao, Y., Liu, J., Xu, Z., & Zhu, D., 2010. Amino-functionalized Fe3O4@ SiO2core-shell magnetic nanomaterial as a novel adsorbent for aqueous heavy metals removal. J. Colloid and Interface Science, 349(1), 293-299.

Wang, W., Kang, R., Yin, Y., Tu, S., & Ye, L., 2022. Two-step pyrolysis biochar derived from agro-waste for antibiotics removal: Mechanisms and stability. J. Chemosphere, 292, 133454.

Wen, J., Xue, Z., Yin, X., & Wang, X., 2022. Insights into an aqueous reduction of Cr (VI) by biochar and its iron-modified counterpart in the presence of organic acids. J. Chemosphere, 286, 131918.

Xiang, J., Lin, Q., Cheng, S., Guo, J., Yao, X., Liu, Q., & Liu, D., 2018. Enhanced adsorption of Cd (II) from aqueous solution by a magnesium oxide–rice husk biochar composite. J. Environmental Science and Pollution Research, 25(14), 14032-14042.

Xiao, Y., Xue, Y., Gao, F., & Mosa, A., 2017. Sorption of heavy metal ions onto crayfish shell biochar: effect of pyrolysis temperature, pH and ionic strength. J. the Taiwan Institute of Chemical Engineers, 80, 114-121. 2.

Yadav, M., Singh, G., & Jadeja, R. N., 2021. Physical and chemical methods for heavy metal removal. J. Pollutants and Water Management: Resources, Strategies and Scarcity, 377-397.

Yang, L., Wu, S., & Chen, J. P., 2007. Modification of activated carbon by polyaniline for enhanced adsorption of aqueous arsenate. J. Industrial & Engineering Chemistry Research, 46(7), 2133-2140.

Yin, G., Tao, L., Chen, X., Bolan, N. S., Sarkar, B., Lin, Q., & Wang, H., 2021. Quantitative analysis on the mechanism of Cd2+ removal by MgCl2-modified biochar in aqueous solutions. J. Hazardous Materials, 420, 126487.

Yin, Q., Wang, R., & Zhao, Z., 2018. Application of Mg–Al-modified biochar for simultaneous removal of ammonium, nitrate, and phosphate from eutrophic water. J. Cleaner Production, 176, 230-240.

Zhao, B., O'Connor, D., Zhang, J., Peng, T., Shen, Z., Tsang, D. C., & Hou, D., 2018. Effect of pyrolysis temperature, heating rate, and residence time on rapeseed stem-derived biochar. J. Cleaner Production, 174, 977-987.

Zhou, Y., GAO, B., Zimmerman, A. R., Chen, H., Zhang, M., & Cao, X., 2014. Biochar-supported zero-valent iron for removal of various contaminants from aqueous solutions. J. Bioresource technology, 152, 538-54.